Sub- and Super-Synchronous Interactions Between STATCOMs and Weak AC/DC Transmissions With Series Compensations

Dewu Shu, *Student Member, IEEE*, Xiaorong Xie, *Senior Member, IEEE*, Hong Rao, *Senior Member, IEEE*, Xiaodan Gao, *Student Member, IEEE*, Qirong Jiang, *Member, IEEE*, and Ying Huang

***Abstract*—With the increasing integration of power electronic converters into the power system, the interactions between converters and their adjacent transmissions bring emerging oscillation issues. A new type of sub- and super-synchronous interactions (S^2SI) between STATCOMs and the weak AC/DC grid were detected in China Southern Grid. As an oscillation incident never reported before, as far as the authors know, its characteristics were quite different from the previous ones. Field measurements as well as simulation studies have revealed that the various factors contributing to the S^2SI include the number of online STATCOMs, the strength of the AC system (in terms of effective short-circuit ratio), the status of series compensation, and the loading level of the HVDC. The mechanism of such oscillation has been clarified and it is caused by the S^2SI between STATCOMs and weak AC grids, where sub- and super-synchronous components are involved in a coupled way. To fully represent such a coupling effect, the concept of sub- and super-synchronous coupled impedance model (IM), or S^2SC-IM, is proposed and developed in order to establish a stability criterion for the S^2SI. Based on the IM-based method as well as the time-domain simulations, the impacts on S^2SI from the various factors are quantitatively analyzed. The results show good consistence among theoretical analysis, electromagnetic simulations, and field measurements. Therefore, the effectiveness of the developed models and the stability criterion has been well verified.**

***Index Terms*—Coupling effects, impedance model (IM), power oscillation, STATCOM, sub- and super-synchronous interaction (S^2SI).**

Manuscript received April 27, 2017; revised August 3, 2017 and September 21, 2017; accepted October 30, 2017. Date of publication November 2, 2017; date of current version June 22, 2018. This work was supported in part by the National Key Research and Development Program of China under Grant 2017YFB0902002, in part by the National Natural Science Foundation of China under Grant 51737007, and in part by the Scientific Project of China Southern Grid under Grant WY-KJXM-20150907. Recommended for publication by Associate Editor J. Liu. *(Corresponding author: Xiaorong Xie.)*

D. Shu, X. Xie, and Q. Jiang are with the State Key Laboratory of Power System, Department of Electrical Engineering, Tsinghua University, Beijing 100084, China (e-mail: shudw13@mails.tsinghua.edu.cn; xiexr@tsinghua.edu.cn; qrjiang@tsinghua.edu.cn).

H. Rao and Y. Huang are with the Electrical Power Research Institute, China Southern Power Grid Company, Guangzhou 510530, China (e-mail: raohong@csg.cn; huangying@csg.cn).

X. Gao is with the Centre for Intelligent Electricity Networks, The University of Newcastle, Callaghan NSW 2308, Australia (e-mail: xiaodan.gao@uon.edu.au).

Color versions of one or more of the figures in this paper are available online at http://ieeexplore.ieee.org.

Digital Object Identifier 10.1109/TPEL.2017.2769702

I. Introduction

POWER oscillation is an important aspect of power system stability. Typical oscillation phenomena includes low-frequency (0.1–2.5 Hz) oscillations among generators [1]–[4], and subsynchronous oscillations (SSO) between turbine generators and adjacent series compensations or HVDC transmissions. These oscillations, mostly caused by the interactions between rotary generators and the transmission grid, have been well studied over the past decades. However, with the increasing integration of power electronic converters into the system, the interactions between converters and their connected transmissions are bringing new oscillation issues, for instance, the harmonic oscillations among multiple converters and the grid [5]–[6], and the emerging SSO between wind farms and the series-compensated transmissions [9]–[10].

As indicated in [11]–[14], high-frequency harmonic oscillations were caused by the coupling of phase lock loops (PLLs), the resonance of filter circuits, or improper parameters of the converter controller. The situation becomes even worse as the number of converters increases. Pietilainen *et al.* [15] and Huang *et al.* [16] discovered that harmonic oscillations can be activated by either the outer DC-link voltage controllers or the inner current controllers. As for the SSO associated with wind farms, there are two potential reasons [17]–[20]: first, the interactions between the converter controllers and a weak AC grid would result in un-damped subsynchronous modes; and second, the controllers of wind generators provide negative damping for the electrical oscillation of a series-compensated grid. It has been revealed that not only the topology and parameters of the grid but also the configuration and control strategies of the converters have great impact on the characteristics of these emerging oscillations [21]–[22].

Recently, a different oscillation phenomenon was detected in a transmission system of China Southern Grid (CSG), where the hydropower is transferred through a corridor consisting an *LCC*-HVDC, series-compensated AC lines and various STATCOMs in the middle. Under certain conditions, both voltages and currents were found to contain obvious subsynchronous (2.5 Hz) and complementary super-synchronous (97.5 Hz) components. In other words, there are sub- and super-synchronous oscillations in the voltages and currents, which then lead to the saturation of STATCOMs' output and the imbalance of reactive power.

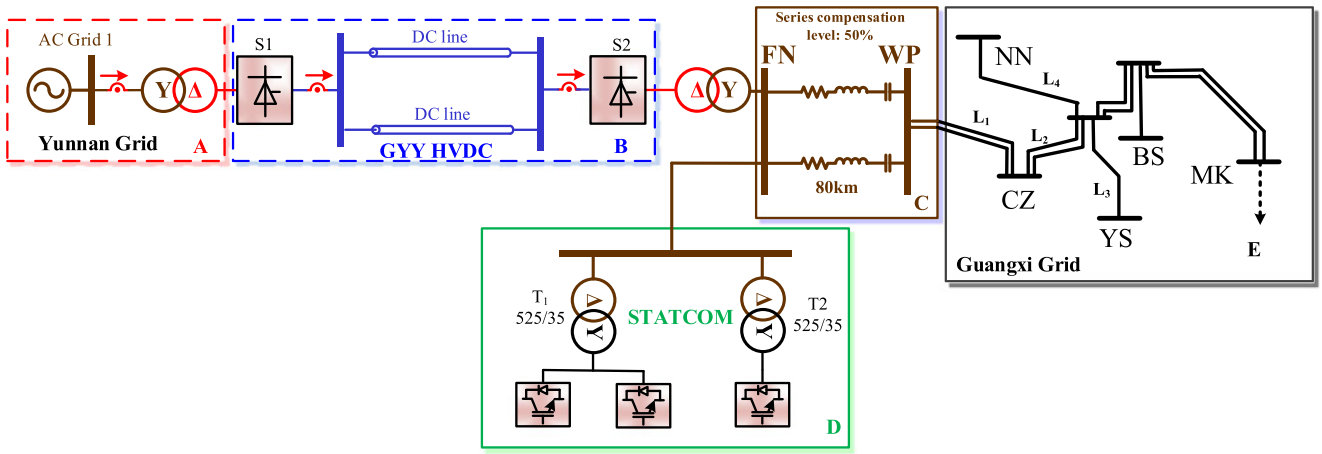

Fig. 1. Single-line diagram of the target system.

However, field measurements and tests indicate that such oscillations do not exist in the previously reported events, and thus, theoretical analysis is required to explain this new phenomenon. Actually, the oscillations are mainly caused by the dynamic interactions between STATCOMs and the weak AC grids with sub- and super-synchronous components involved in a coupled way, which the authors called "sub- and super-synchronous interaction (S^2SI)."

This paper is aimed to investigate the mechanism and characteristics of the said S^2SI. The contributions are summarized as follows.

1) The path of oscillation and the participants of S^2SI have been identified based on field measurements. The influence of HVDC is also revealed.
2) A real-world oscillation incident is reproduced with time-domain simulations, whereby the impacts on S^2SI from several factors, including the number of online STATCOMs, the status of series compensations, the power of HVDC, and the strength of the AC system in terms of effective short-circuit ratio (ESCR) have been investigated in detail.
3) Furthermore, the sub- and super-synchronous coupled impedance model (S^2SC-IM) is proposed and developed to establish a stability criterion for the S^2SI. Thus, the mechanism of this new oscillation is clarified and its characteristics can be quantified.

The rest of this paper is organized as follows: Section II presents the target system and its actual S^2SI events. In Section III, a typical S^2SI event is reproduced through time-domain simulations, whereby the impacts from various factors are also discussed. Section IV develops the stability criterion based on S^2SC-IM and further analyzes the characteristics of the S^2SI. Section V concludes the paper.

II. Desriptions of the System and Oscillation Events

A. Description of the System

As shown in Fig. 1, the hydropower of Yunnan Grid (Part A, in the west of CSG) is transferred eastward to Guangxi Grid (Part E, in the center of CSG) through the GYY HVDC (Part B) and the series-compensated AC transmissions (Part C). The HVDC has a rated DC voltage of ± 500 kV and a rated capacity of 3000 MW. Since the inverter station, namely FN, is remote from the receiving end, the ESCR at the AC bus of FN station is as small as 2.05, much less than the normally required value for a well-planned system, for instance 3.0 [24]. In other words, the HVDC is connected to a very weak AC terminal. To strengthen the electrical tie and ensure transient stability, the parallel AC transmission lines are series compensated with a compensation level of 50%. Here, the compensation level of a transmission line is defined as the ratio of the capacitive impedance of the series capacitors to the inductance impedance of the line, all in the fundamental frequency [25]. Moreover, three identical STATCOMs, each with a rating of 100 Mvar, are deployed at FN station to support the bus voltage (see Part D in Fig. 1). Usually, the STATCOMs are operated at the mode of constant reactive power output.

B. Actual S^2SI Events

Under-damped oscillations had been frequently observed since the STATCOMs were put into service. Originally, the operators guessed that the oscillations were caused by the sub-synchronous torsional interaction (SSTI) related to the series compensations [18]. However, as the series capacitors were deliberately bypassed by the operators, the oscillations still occurred. Extensive field measurements indicated that only all or parts of STATCOMs were out of service, the oscillations disappeared. So the STATCOMs play a crucial role in the formation of the oscillations.

A typical oscillation event is illustrated here to detail the S^2SI. Just before the oscillation accident, the HVDC was operated at a very low loading level (10% of its rated power, or 300 MW) and all its AC filter banks were out of service. One of the two transmission lines from FN to WP (Part C) was temporarily out of service due to scheduled maintenance, which made the AC system even weaker. Initially (corresponding to the time less than 1 s in Figs. 2–4), only one STATCOM (#1) was online. The system was normal until a second STATCOM (#2) was put into operation at $t = 1$ s, when the oscillation appeared. At this

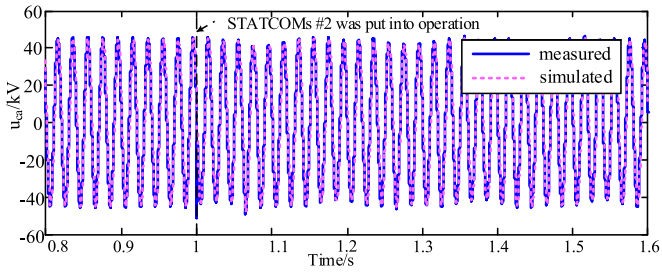

Fig. 2. Voltages at the FN bus.

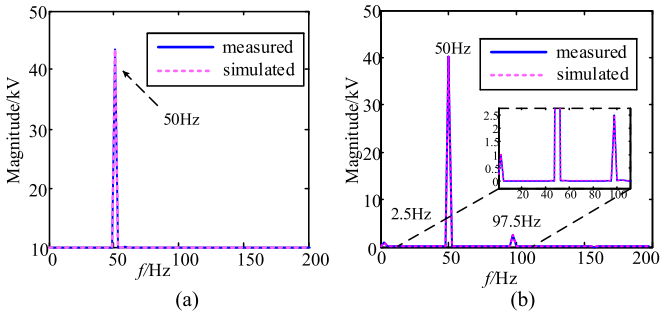

Fig. 3. Spectrum of the voltages at the FN bus (a) just before the oscillation event; (b) during the oscillation event.

time, each of the two STATCOMs had an average fundamental var output of -40 Mvar. The oscillation amplitude of i_{qr} then increased dramatically due to the oscillation. It reached the lower boundary of -1.0 p.u. and the controllers of STATCOM saturated to a shallow extent, resulting in sustained oscillations in the system. Figs. 2–5 display the waveforms of the voltages and currents, together with their spectrums during the event.

From these field measurements, it can be observed that the bus voltages as well as the currents of the STATCOMs and the AC line contain obvious subsynchronous (2.5 Hz) and complementary super-synchronous (97.5 Hz) components. It is of particular concern that the super-synchronous component is over twice the subsynchronous component [see Figs. 3(b) and 5]. Since it is quite different from the traditional SSTI, where subsynchronous interharmonics dominate, this oscillation is named as the S^2SI to highlight the coupling effect of sub- and super-synchronous components. Furthermore, the spectrum of the currents flowing though the HVDC, the AC line, and the STATCOMs are obtained as shown in Fig. 5. It can be seen that their relative magnitudes are 7%, 93%, and 100%, respectively. In other words, the sub- and super-synchronous currents of the STATCOMs are the sum of those of the HVDC and the AC line. Since the HVDC accommodates a very small percent of the sub- and super-synchronous currents, it barely participates into the S^2SI. Therefore, it can be concluded that the oscillations are dominated by the dynamic interactions between the STATCOMs and the AC grid. Fig. 4(d) noticeably shows that the S^2SI happened before the q-axis current reference of the STATCOM, or i_{qr}, reached its lower boundary. Then as i_{qr} became saturated shallowly due to the hard limit, the oscillation remained sustained.

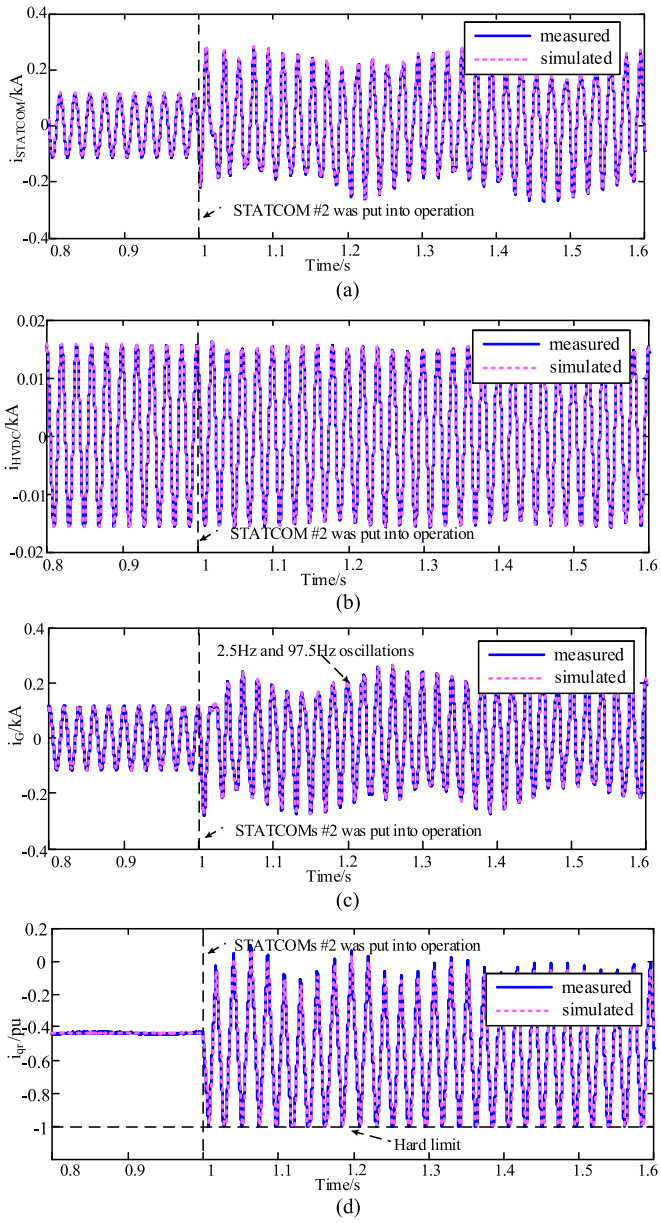

Fig. 4. (a) currents of STATCOM # 1; (b) currents of HVDC; (c) currents of the line from FN to WP; (d) q-axis current reference (i_{qr}) of STATCOM # 1.

III. Time-Domain Simulation Based Analyses

In this section, the above-mentioned S^2SI event will be reproduced with the electromagnetic transient (EMT) model of the target system. Thus, a deep investigation of its characteristics and influential factors could be performed based on the detailed simulations.

A. EMT Model of the Target System

The EMT model of the target system in Fig. 1 is established using the software PSCAD/EMTDC with a simulation step of 20 μs. The EMT models of STATCOMs and HVDC converters are provided by the manufacturers as "black-boxes" due to the consideration of business secrets. The main grid of the AC

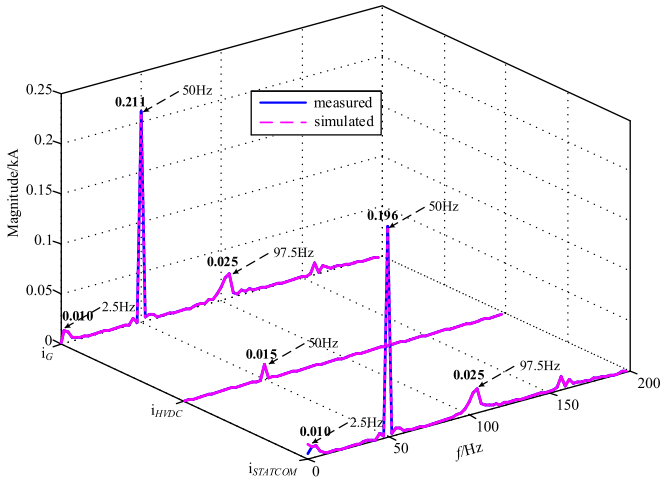

Fig. 5. Spectrum of the currents of STATCOM #1 (i_{STATCOM}), HVDC (i_{HVDC}), and the FN-WP line (i_G).

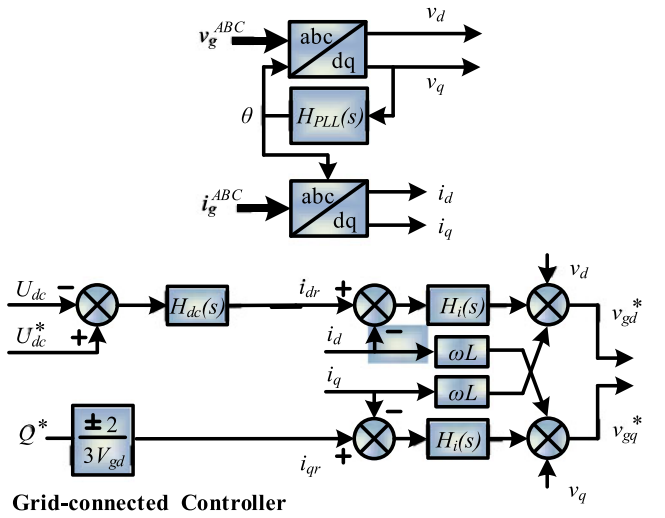

Fig. 6. Control scheme of STATCOM.

TABLE I
PARAMETERS OF THE RELEVANT LINES AND TRANSFORMERS

Part	Parameter	Value (p.u.)	Parameter	Value (p.u.)
C	r_L	0.00078	x_C	0.00487
	x_L	0.00977	Comp. level	50%
D	x_{T1}	0.12000	x_{T2}	0.12000
E	r_{L1}	0.00051	x_{L1}	0.00660
	r_{L2}	0.00103	x_{L2}	0.01291
	r_{L3}	0.00103	x_{L3}	0.01291
	r_{L4}	0.00128	x_{L4}	0.01809
	r_L (MK)	0.00173	x_L (MK)	0.10946
	r_L (BS)	0.00561	x_L (BS)	0.13215

Note: Base voltage = 525 kV; Base capacity = 100 MVA

TABLE II
CIRCUIT PARAMETERS AND CONTROL PARAMETERS OF STATCOMS

	Name	Value
Circuit Parameters	PCC nominal current (peak):I_g	2.355 kA
	PCC nominal voltage (peak):V_g	49.49 kV
	Steady state output current: i_{dq}	(0.01-j*0.4518) p.u.
	Steady state output voltage: v_{dq}	(0.914-j*0.0084) p.u.
Control Parameters	PLL-proportional gain: K_{pll}	50 rad/s
	PLL-integral gain: K_{ipll}	900 rad/s^2
	Proportional gain of DC voltage controller: K_{pdc}	1.6 Ω^{-1}
	Integral gain of DC voltage controller: K_{idc}	0.002 Ω^{-2}
	Proportional gain of current controller: K_{pi}	1.0 Ω
	Integral gain of current controller: K_{ii}	1.0 Ω/s

system is kept and the actual parameters of transmissions are adopted. Table I lists the parameters of the relevant AC lines and the 35/525 kV transformers connecting the STATCOMs. The transmission lines are represented by the well-known PI-section models, including a series *R-L* branch and two shunt capacitive branches. Generally, the shunt capacitances have little effect on the said S^{2}SI and thus can be ignored. The loads at buses MK and BS are modeled as *R-L* branches, with their parameters (r_L and x_L) also listed in Table I. The STATCOM is an IGBT-based voltage-source converter with the chain-circuit topology. Each phase has 50 full-bridge submodules and an interface inductor of 7 mH. The capacitance of each submodule is 6500 μF. The control scheme of STATCOM is illustrated in Fig. 6, where v_g^{ABC} and i_g^{ABC} are the AC voltages and currents at the point of common coupling (PCC). All STATCOMs have the same configuration, electrical parameters, and control schemes. The inner loop is the current tracking control in the $d-q$ reference frame. There are two outer control loops: the DC voltage control to maintain the voltages of DC links, and the reactive power control to drive the STATCOM to generate the preset var. The major parameters of STATCOMs are listed in Table II. During the oscillation event, the sending end of the GYY HVDC operated as a rectifier to maintain the power or DC current; whereas the receiving end operated in the extinction-angle-control mode.

In the simulation model, the initial state is established according to the power flow of the actual system condition. Next, STATCOM #2 is switched ON just as the real system had experienced. Then, similar oscillation is observed as the simulation goes on. Finally, the simulation results are plotted against the field measurements, as shown in Figs. 2–5. Obviously, they coincide very well. In other words, the actual S^{2}SI event is reproduced with the simulation model, which thus can be used to examine how the characteristics of oscillation are affected by the various factors, especially the status of STATCOM, series compensation, HVDC, and the strength of the AC system.

B. *Influential Factors and Their Impacts on S^{2}SI*

1) Number and var Output of Online STATCOMs: The number of online STATCOMs has a crucial impact on the S^{2}SI, which has been demonstrated by both field measurements and EMT simulations (see Figs. 2–5). When there is no or only one STATCOM in service, the oscillation does not appear. However, if two or more STATCOMs are brought into service, S^{2}SI would be triggered under some operating conditions, especially when the AC grid is weakened for some reasons.

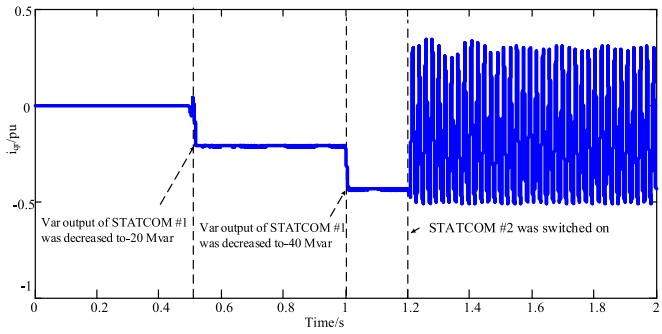

Fig. 7. The q-axis current reference (i_{qr}) of STATCOM #1 under different reactive power outputs.

EMT simulations have been carried out to investigate how the occurrence of S^{2}SI is affected by the number and var output of online STATCOMs. Typical results are shown in Fig. 7. Before the time $t = 1.2$ s, only STATCOM #1 is online and its initial output is zero. At the time of 0.5 and 1.0 s, the var output is decreased to -20 and -40 Mvar, respectively. At $t = 1.2$ s, a second STATCOM is switched ON. However, the total var output is still kept at -40 Mvar to maintain a comparable situation of the grid. As can be seen, the decrease of reactive power (Q) would not trigger oscillation. It is not until a second STATCOM (#2) is put into operation at $t = 1.2$ s that the oscillation appears. This scenario clearly shows that the occurrence of the S^{2}SI oscillation is more related to the number of online STATCOMs than the var output of each STATCOM. The latter has little impact on the occurrence of the oscillation. These results coincide well with field observations.

2) Series Compensation: The influence of the series compensations is illustrated by simulating the following scenario: the sustained oscillation is first reproduced with series compensations in service, and then at $t = 1$ s, they are bypassed deliberately to check how the oscillation will be changed. The simulation results are displayed in Fig. 8. Obviously, the oscillation does not disappear. After a short transient period, there is still a sustained oscillation, however, with different amplitude and frequency. The subsynchronous (super-synchronous) frequency is increased (decreased) from 2.5 (97.5) Hz to 10 (90) Hz, whereas the amplitudes of both sub- and super-synchronous current become a little bit higher. In other words, the switching ON/OFF of series compensations would not determine the existence or nonexistence of S^{2}SI, but just change its magnitude and frequency.

3) Variation of HVDC Power: Similar simulation studies are carried out with a variation of the HVDC power. Fig. 9 shows the currents and their spectrums before and after a sudden decrease of the DC power from 300 to 100 MW at $t = 1$ s. It can be seen that the oscillation frequency remains the same. Only the amplitude changes vary a little. More simulation cases also indicate that the variation of the HVDC power has little impact on the frequency but a slight impact on the amplitude of the oscillation.

4) Strength of the AC Grid: The strength of the system is usually quantified with the term of ESCR, which is defined

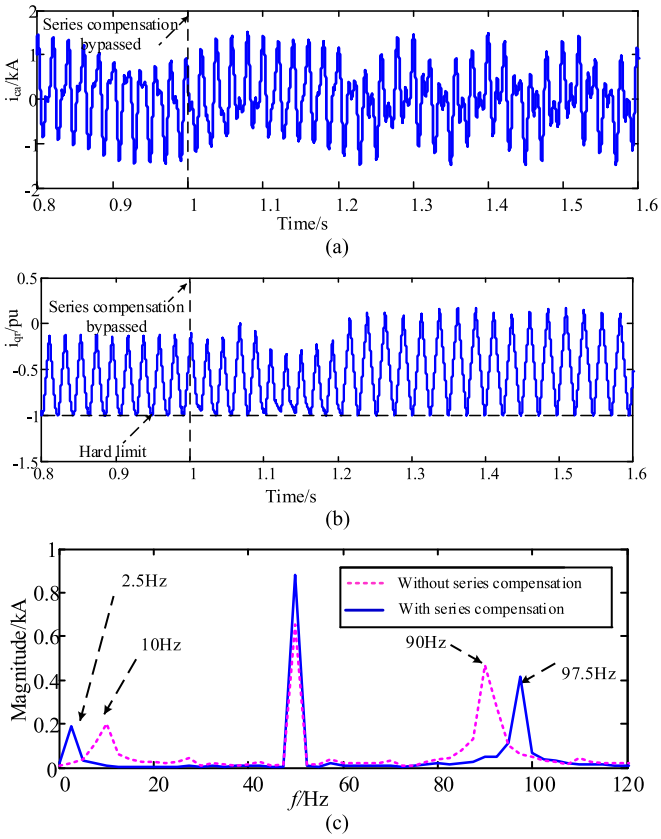

Fig. 8. Impact of switching ON/OFF series compensations on S^{2}SI: (a) currents of STATCOMs; (b) the q-axis current reference (i_{qr}) of STATCOM #1; (c) spectrum of the current of STATCOM.

as [26], [27]

$$\text{ESCR} = \frac{S_{sc} - Q_{cN}}{P_{dN}} \tag{1}$$

where S_{sc} is the short-circuit capacity of the AC system; Q_{cN} is the total rated reactive power generated by AC filters and other reactive power sources (including STATCOMs); P_{dN} is rated power of the HVDC transmission.

Generally, the length or reactance of transmission lines affects the short-circuit capacity to a great extent. Thus, by simulating the different cases with varied lengths of the FN-WP line, the authors can study the impact on S^{2}SI from the strength of the AC grid. The results of a typical case are shown in Fig. 10, where the length of the FN-WP line is suddenly changed from the original 80 km (ESCR $= 2.05$) to 20 km (ESCR $= 3.6$) at $t = 1$ s. Obviously, the oscillation disappears immediately after such an increase of ESCR. This and other cases have concluded that the risk of oscillation could be decreased by increasing the strength of the AC grid.

IV. Impedance Model Based Analyses

A. Sub- and Super-Synchronous Coupled Impedance Model

As demonstrated, the stated S^{2}SI events are mainly caused by the dynamic interactions between the voltage-sourced-converter (VSC) based STATCOMs and the weak AC grid. For the char-

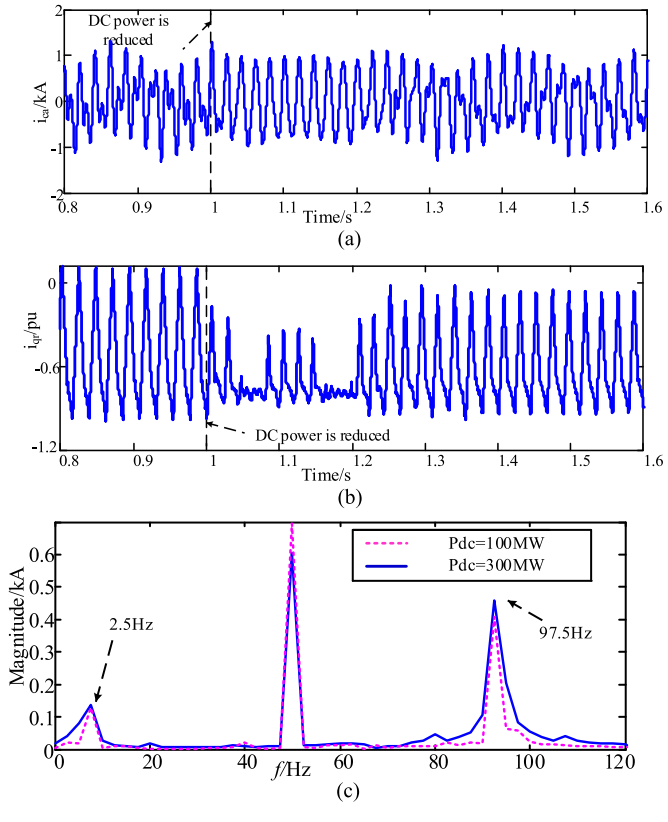

Fig. 9. Impact of varying the DC power on S^{2}SI: (a) currents of STATCOMs; (b) the q-axis current reference (i_{qr}) of STATCOM #1; (c) spectrum of the current of STATCOM.

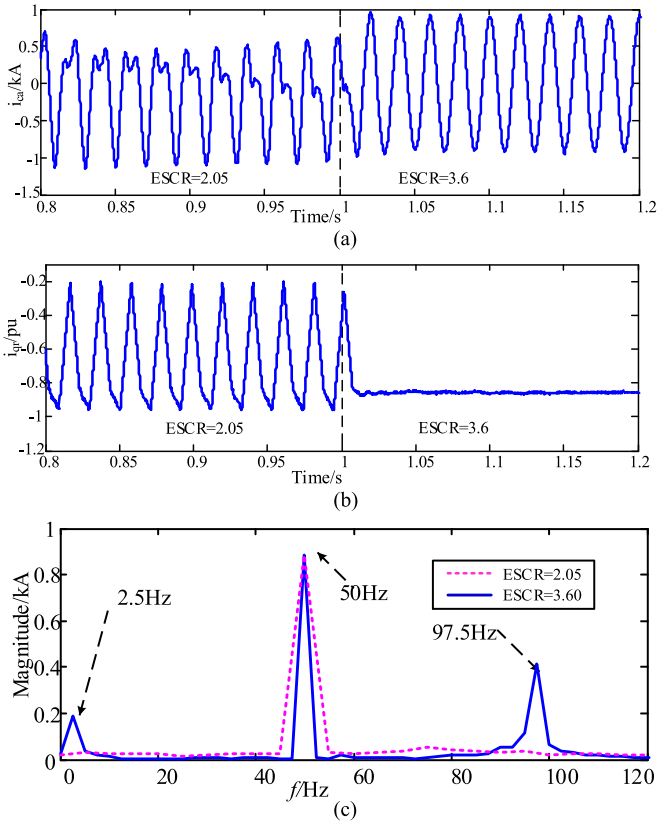

Fig. 10. Impact of increasing ESCR on S^{2}SI : (a) currents of STATCOMs; (b) the q-axis current reference (i_{qr}) of STATCOM #1; (c) spectrum of the current of STATCOM.

acteristic analyses of such power-electronic-converter participated interactions, impedance models (IMs) are widely used for analyses for high-frequency oscillations of converters, for instance, those IMs presented in [28]–[32]. Different from the high-frequency oscillations mentioned in [30]–[32], in the oscillation incidents experienced by CSG, the sub- and super-synchronous components of the voltages and currents always appeared in a strongly coupled way. In other words, when the converters (e.g., STATCOM and HVDC) are perturbed by a subsynchronous voltage (current), they would output current (voltage) components not only at the same subsynchronous frequency but also at the complementary super-synchronous frequency, and vice visa. Actually, the coupling effects are induced by the dq/abc transformation (and/or PLL) inherent in the converter, which always transforms a component at the frequency of ω ($\omega < \omega_0$) in the dq frame into two components simultaneously in the abc frame. One is at the subsynchronous frequency of $\omega_0 - \omega$; whereas the other is at the complementary super-synchronous frequency of $\omega_0 + \omega$, where ω_0 is the rated system frequency [22], [31]–[35]. Such coupling effects have also been noticed in [33]. The previous work focused more on the development of a generalized modeling framework. Here, the couplings between complimentary frequencies are observed in practical oscillation events, providing an actual verification of the theoretical derivation.

The concept of S^{2}SC-IM is proposed in this paper to reflect the coupling effects. Mathematically, it can be derived from the previous theoretical work [37], according to which, the small-signal behavior of a converter in the sequence domain can be described by an impedance matrix as

$$\begin{bmatrix} U_p(s+j\omega_0) \\ U_n(s-j\omega_0) \end{bmatrix} = \begin{bmatrix} Z_{pp}(s) & Z_{pn}(s) \\ Z_{np}(s) & Z_{nn}(s) \end{bmatrix} \begin{bmatrix} I_p(s+j\omega_0) \\ I_n(s-j\omega_0) \end{bmatrix} \tag{2}$$

where $U_p(s)$ and $U_n(s)$ are the positive/negative voltages; $I_p(s)$ and $I_n(s)$ are the positive/negative currents; $Z_{ij}(s), i, j = p, n$ denote the self- and mutual impedances between positive- and negative- sequence components, all in s-domain.

The voltages in the dq domain can be calculated from $U_p(s)$ and $U_n(s)$ as [37]

$$U_{dq}(s) = U_p(s)e^{(s-j\omega_0)t} + U_n^*(s)e^{(s^*+j\omega_0)t} \tag{3}$$

where ω_0 is the rated system frequency; the symbol * denotes the complex conjugate.

Therefore, the voltages in the xy (stationary) domain can be obtained by multiplying $e^{j\omega_0 t}$ to (3), or

$$U(s) = U_{dq}(s)e^{j\omega_0 t} = U_p(s)e^{st} + U_n^*(s)e^{(s^*+j2\omega_0)t}. \tag{4}$$

Considering only the positive currents and substituting (4) into (2), the voltage in the stationary domain, i.e., $U(s)$ is given by

$$\begin{aligned} U(s) &= U_{dq}(s)e^{j\omega_0 t} \\ &= Z_{pp}(s-j\omega_0)I_p(s)e^{st} \\ &\quad + Z_{np}(s^*+j\omega_0)I_p^*(s)e^{(s^*+j2\omega_0)t} \\ &= Z_{pp}(s-j\omega_0)I(s) \\ &\quad + Z_{np}(s^*+j\omega_0)e^{j2\omega_0 t}I^*(s^*) \end{aligned} \tag{5}$$

where $I(s) = I_p(s)e^{st}$.

The conjugate of (5) is

$$\begin{aligned} U^*(s^*)e^{j2\omega_0 t} = Z_{pp}^*(s^*+j\omega_0)e^{j2\omega_0 t}I^*(s^*) \\ + Z_{np}(s-j\omega_0)I(s). \end{aligned} \tag{6}$$

The final S^{2}SI-IM in s domain, namely $Z_{\rm ssc}(s)$, is the combination of (5) and (6), or

$$\begin{aligned} &\begin{bmatrix} U(s) \\ U^*(s^*)e^{j2\omega_0 t} \end{bmatrix} \\ &\quad = \begin{bmatrix} Z_{pp}(s-j\omega_0) & Z_{np}(s^*+j\omega_0) \\ Z_{np}(s-j\omega_0) & Z_{pp}^*(s^*+j\omega_0) \end{bmatrix} \\ &\qquad \times \begin{bmatrix} I(s) \\ I^*(s^*)e^{j2\omega_0 t} \end{bmatrix} \\ &\quad = Z_{\rm ssc}(s) \begin{bmatrix} I(s) \\ I^*(s^*)e^{j2\omega_0 t} \end{bmatrix}. \end{aligned} \tag{7}$$

Letting $s = j\omega_d (\omega_d < \omega_0)$, the S^{2}SI-IM in the frequency domain can be derived by using the phasor representations [31]:

$$\begin{aligned} \begin{bmatrix} \dot{U}(j\omega_{\rm d}) \\ \dot{U}_c^*(j\omega_{\rm d,c}) \end{bmatrix} &= Z_{\rm ssc}(j\omega_{\rm d}) \begin{bmatrix} \dot{I}(j\omega_{\rm d}) \\ \dot{I}_c^*(j\omega_{\rm d,c}) \end{bmatrix} \\ &= \begin{bmatrix} z_{11}(j\omega_{\rm d}) & z_{12}(j\omega_{\rm d}) \\ z_{21}(j\omega_{\rm d}) & z_{22}(j\omega_{\rm d}) \end{bmatrix} \begin{bmatrix} \dot{I}(j\omega_{\rm d}) \\ \dot{I}_c^*(j\omega_{\rm d,c}) \end{bmatrix} \end{aligned} \tag{8}$$

where $\omega_{\rm d,c} = 2\omega_0 - \omega$ is the complimentary super-synchronous frequency; $\dot{I}(j\omega_{\rm d})$, $\dot{I}_c^*(j\omega_{\rm d,c})$, and $\dot{U}(j\omega_{\rm d})$, $\dot{U}_c^*(j\omega_{\rm d,c})$ are the phasors of their corresponding frequencies; $z_{ii}(j\omega_d)$ $(i = 1, 2)$ are self-impedances, indicating the relationship between the sub- or super-synchronous voltage with the current at the same frequency; and $z_{ij}(j\omega_{\rm d})$ $(i, j = 1, 2, i \neq j)$ are mutual-impedances, standing for the couplings between the sub- or super-synchronous voltage with the current at the complementary frequency.

It should be noted that there are two frequencies, i.e., $\omega_{\rm d}$ and $\omega_{\rm d,c}$, in the IM. Since $\omega_{\rm d,c}$ depends on $\omega_{\rm d}$, $z_{ij}(j\omega_{\rm d})$ $(i, j = 1, 2)$ is determined by the variable $\omega_{\rm d}$ and the constant ω_0. Similar to the definition given in [32]–[37], the elements of the S^{2}SI-IM or $z_{ij}(j\omega_{\rm d})$ $(i, j = 1, 2)$ are defined in the same way as the conventional concept of complex impedance used for the phasor representation in circuit theory. They are just mathematical representations of the relationship between two phasors, specified by

$$\begin{cases} z_{11}(j\omega_{\rm d}) = \frac{|U(j\omega_{\rm d})|}{|I(j\omega_{\rm d})|}\angle\left[\angle U(j\omega_{\rm d}) - \angle I(j\omega_{\rm d})\right] \\ z_{12}(j\omega_{\rm d}) = \frac{|U(j\omega_{\rm d})|}{|I_c(j\omega_{\rm d,c})|}\angle\left[\angle U(j\omega_{\rm d}) + \angle I_c(j\omega_{\rm d,c})\right] \\ z_{21}(j\omega_{\rm d}) = \frac{|U_c(j\omega_{\rm d,c})|}{|I(j\omega_{\rm d})|}\angle\left[-\angle U_c(j\omega_{\rm d,c}) - \angle I(j\omega_{\rm d})\right] \\ z_{22}(j\omega_{\rm d}) = \frac{|U_c(j\omega_{\rm d,c})|}{|I_c(j\omega_{\rm d,c})|}\angle\left[-\angle U_c(j\omega_{\rm d,c}) + \angle I_c(j\omega_{\rm d,c})\right] \end{cases} \tag{9}$$

where $|\cdot|$ and $\angle\cdot$ denote the magnitude and phase angle of the enclosed phasors.

The S^{2}SC-IM (8) is primarily defined to reflect the couplings between sub- and super-synchronous components in converters, specifically the STATCOM and HVDC in this paper. Naturally, if the mutual impedances are negligible as compared to the self-impedances, the 2×2 impedance matrix can be reduced into a decoupled IM, which is exactly the same as the existing concept of IM. For some other devices, for instance the transmission lines and the transformers, the mutual impedances are zeroes, which results in non-coupled IMs.

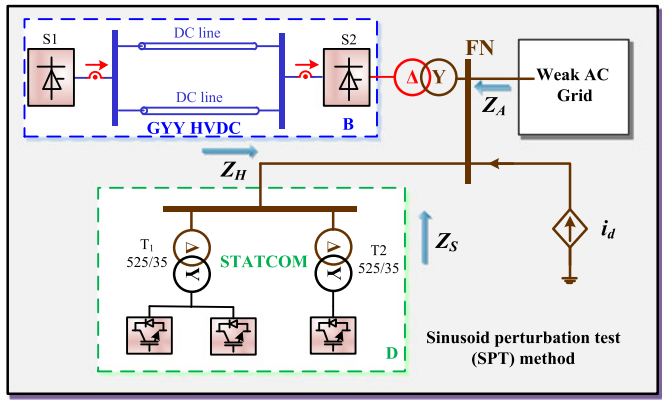

Fig. 11. Illustration of the measurement of S^2 SC-IM using sinusoidal perturbation tests.

B. Measurement of S^{2}SC-IM Using Sinusoidal Perturbation Tests

The target system in Fig. 1 is divided at the bus of FN into three subsystems, namely:

1) STATCOM: including all STATCOMs with their controllers and interface transformers;
2) HVDC: including the HVDC transmission and its sending-end AC system;
3) AC grid: including the AC transmissions to the right of bus FN.

Each subsystem can be represented by an S^{2}SC-IM connected to the common bus of FN, as illustrated in Fig. 11.

Theoretically, the S^{2}SC-IM of each subsystem could be derived provided that its topological configuration, control scheme, and parameters are available. However, the manufacturers of STATCOM and HVDC would not release the detailed information due to the consideration of business secrets. They

only provided "black-box" modules for the purpose of simulation studies. Therefore, the IMs of STATCOMs and HVDC converters can only be obtained using input-output model identification. So the sinusoid perturbation test (SPT) method is used to identify the frequency-dependent model for the stability analysis [22]. The principle of SPT is illustrated in Fig. 11. When the system is under a stable and steady state in the EMT simulation model, the following three-phase balanced sinusoid currents are injected into the bus of FN as a small perturbation to the system:

$$\begin{cases} i_{d,a}(t) = I_d\cos(\omega_d t + \phi) \\ + I_{d,c}\cos(\omega_{d,c} t + \phi_c) \\ i_{d,b}(t) = I_d\cos(\omega_d t - 2/3\pi + \phi) \\ + I_{d,c}\cos(\omega_{d,c} t - 2/3\pi + \phi_c) \\ i_{d,c}(t) = I_d\cos(\omega_d t + 2/3\pi \\ + \phi) + I_{d,c}\cos(\omega_{d,c} t + 2/3\pi + \phi_c) \end{cases} \tag{10}$$

where I_d and $I_{d,c}$ are the amplitudes of the subsynchronous and the complementary super-synchronous currents, which should be properly set in order to excite the required dynamics sufficiently without introducing nonlinearities; ω_d ($< \omega_0$) is the subsynchronous frequency and $\omega_{d,c} = 2\omega_0 - \omega_d$ corresponding to the complimentary super-synchronous frequency; ϕ and ϕ_c are initial phases.

Then, the terminal voltages and currents of all subsystems are collected from the simulation results. With some signal manipulations, their sub- and super-synchronous components are extracted from collected data. Thus, the following equations, which are adapted from (8), could be established for each subsystem:

$$\begin{cases} \dot{U}(j\omega_{\rm d}) = \dot{I}(j\omega_{\rm d}) z_{11}(j\omega_{\rm d}) + \dot{I}_c^*(j\omega_{\rm d,c}) z_{12}(j\omega_{\rm d}) \\ \dot{U}_c^*(j\omega_{\rm d,c}) = \dot{I}(j\omega_{\rm d}) z_{21}(j\omega_{\rm d}) + \dot{I}_c^*(j\omega_{\rm d,c}) z_{22}(j\omega_{\rm d}) \end{cases} \tag{11}$$

where all voltage/current components and the impedances are expressed in the frequency domain.

Equation (11) has four unknown elements, i.e., $z_{ij}(j\omega_{\rm d})$ $(i,j=1,2)$ but only two equations. So, another SPT should be carried out by just varying the amplitudes of the injected currents as in (10). As a result, another two equations with the same unknown variables are established. Next, the four impedances or the S^{2}SC-IM of each subsystem could be obtained from these equations. Of course, more SPTs would provide more equations. In such cases, the least square algorithm might be used to identify the IMs more accurately.

The above procedure produces the S^{2}SC-IM at the specific frequency-pair of $\omega_{\rm d}$ and $\omega_{\rm d,c}$. By repeating the procedure under different frequencies, the S^{2}SC-IM over a certain range, for instance $\boldsymbol{Z_{\rm ssc}(j\omega_{\rm d})}$, $\boldsymbol{\omega_{\rm d} \in (0, \omega_0)}$ can be obtained for each subsystem.

C. Stability Criterion Based on the S^{2}SC-IM

For the study of S^{2}SI, the target system is represented with three S^{2}SC-IMs or branches connected to a common bus, as shown in Fig. 11. The dynamic modes of the system could be computed from the interconnected IMs. For simplicity, it is assumed that there is a voltage-pair perturbation $\dot{U}_{\rm d}$ and $\dot{U}_{\rm dc}^*$ (both in phasors) injected at the FN bus. According the circuit theory, the current responses at the same place, i.e., $\dot{I}_{\rm d}$ and $\dot{I}_{\rm d,c}$, are given by

$$\begin{bmatrix} \dot{U}_{\rm d} \\ \dot{U}_{\rm d,c}^* \end{bmatrix} = \boldsymbol{Z}_{ssc,\Sigma}(j\omega_{\rm d}) \begin{bmatrix} \dot{I}_{\rm d} \\ \dot{I}_{\rm d,c}^* \end{bmatrix} \tag{12}$$

and $\boldsymbol{Z}_{ssc,\Sigma}(\boldsymbol{j}\omega_{\rm d})$ is the total S^{2}SC-IM, or

$$\begin{aligned} \boldsymbol{Z}_{ssc,\Sigma}(j\omega_{\rm d}) &= \begin{bmatrix} z_{\Sigma 11}(j\omega_{\rm d}) & z_{\Sigma 12}(j\omega_{\rm d}) \\ z_{\Sigma 21}(j\omega_{\rm d}) & z_{\Sigma 22}(j\omega_{\rm d}) \end{bmatrix} \\ &= (\boldsymbol{Z}_H^{-1}(j\omega_{\rm d}) + \boldsymbol{Z}_S^{-1}(j\omega_{\rm d}))^{-1} + \boldsymbol{Z}_A(j\omega_{\rm d}) \end{aligned} \tag{13}$$

where $\boldsymbol{Z}_S(\boldsymbol{j}\omega_{\rm d})$, $\boldsymbol{Z}_H(\boldsymbol{j}\omega_{\rm d})$, and $\boldsymbol{Z}_A(\boldsymbol{j}\omega_{\rm d})$ are the S^{2}SC-IMs of the subsystems of STATCOM, HVDC, and AC grid, respectively.

Mathematically, the decoupled $Z_A(j\omega_{\rm d})$ is expressed in the following form of transfer function:

$$Z_A(j\omega_{\rm d}) = \begin{bmatrix} R + j\omega_{\rm d}L - j/(\omega_{\rm d}C) & 0 \\ 0 & R - j\omega_{\rm d,c}L + j/(\omega_{\rm d,c}C) \end{bmatrix} \tag{14}$$

where $\omega_{\rm d} = \omega (< \omega_0)$ is the subsynchronous frequency and $\omega_{\rm d,c} = 2\omega_0 - \omega$ corresponding to the complimentary super-synchronous frequency; $R, L,$ and C are lumped resistance, inductance, and series-connected capacitance.

Generally, the small-signal stability of the target system depends on the locations of the zeroes of the impedance matrix, i.e., $Z_{\rm ssc}(s)$. If the system is observable and controllable, i.e., the system has no internal pole-zero cancellation, the zeroes of $Z_{\rm ssc}(s)$ are just the zeroes of its determinant, i.e., $D(s)$ [22]–[23].

Let

$$\boldsymbol{D(s)} = \boldsymbol{Det}\{Z_\Sigma(s)\} = z_{\Sigma 11}(s) z_{\Sigma 22}(s) - z_{\Sigma 21}(s) z_{\Sigma 12}(s) \tag{15}$$

$$\boldsymbol{X(s)} = Im\{\boldsymbol{D(s)}\}, \boldsymbol{R(s)} = Re\{\boldsymbol{D(s)}\} \tag{16}$$

where $Det\{\cdot\}$ means the determinant of the enclosed matrix; $Im\{\cdot\}$ and $Re\{\cdot\}$ denote the imaginary and real parts of the enclosed variables; $\boldsymbol{X(s)}$ and $\boldsymbol{R(s)}$ are the reactance and resistance of $\boldsymbol{D(s)}$.

Therefore, the stability of the target system is dependent upon the zeroes of $D(s)$. Specifically, the system is stable when all zeroes have negative real parts, otherwise the system is unstable. Supposing that the zero of $D(s)$ is s^*, or $D(s^*) = 0$, where $s^* = \sigma^* + j\omega^*, \sigma^* \ll \omega^*$, and that there exists an angular frequency $\omega_{\rm ssc} \approx \omega^*$, satisfying $Im\{D(j\omega_{\rm ssc})\} = 0$, thus, there exists a $\delta > 0$, such that, for all $||(\sigma^* + j\omega^*) - j\omega_{\rm ssc}|| < \delta$, the Taylor expansion of $D(s^*)$ at $j\omega_{\rm ssc}$ is given by (17), where $\Delta\omega^* = \omega^* - \omega_{\rm ssc}$, $R(j\omega) = Re\{D(j\omega)\}$, and $X(j\omega) = Im\{D(j\omega)\}$ are the real and

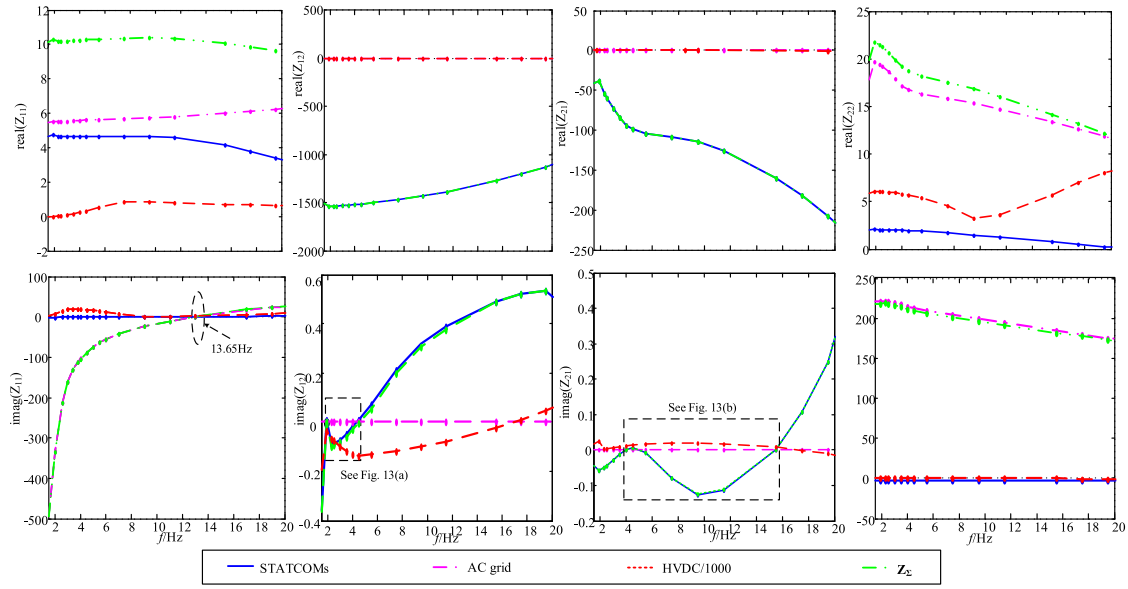

Fig. 12. Impedance—frequency curves of the STATCOMs, the AC grid, the HVDC, and the total impedance.

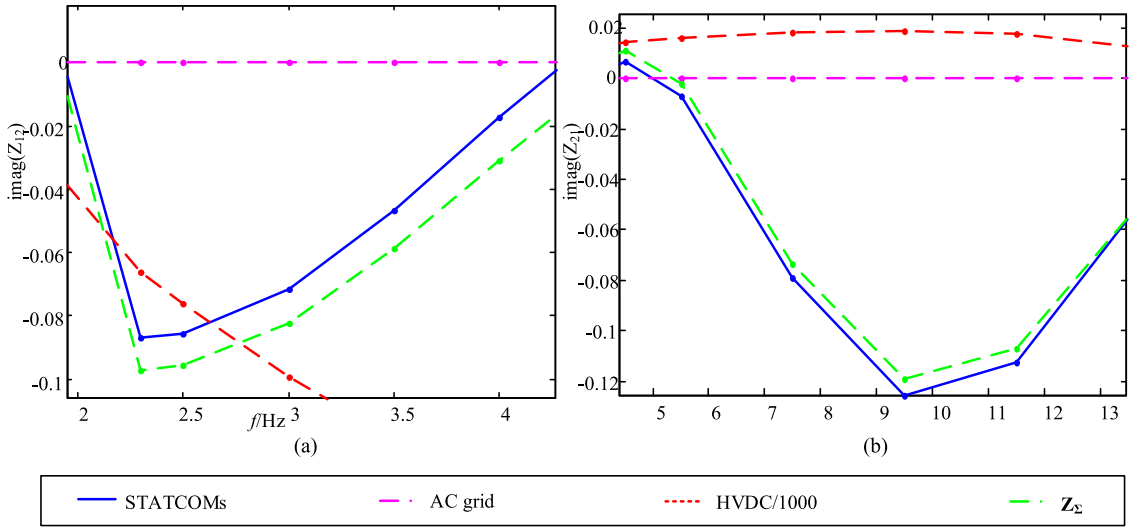

Fig. 13. Enlarged curves of the imaginary parts of $Z_{12}(j\omega_{\mathrm{d}})$ and $Z_{21}(j\omega_{\mathrm{d}})$ in Fig. 12.

imaginary parts

$$
\begin{aligned}
D(s^*) &\approx D(j\omega_{\mathrm{ssc}}) + \left.\frac{dD(s)}{ds}\right|_{s=j\omega_{\mathrm{ssc}}} (\sigma^* + j\Delta\omega^*) \\
&= R(j\omega_{\mathrm{ssc}}) + X(j\omega_{\mathrm{ssc}}) + \left.\frac{dD(j\omega)}{d(j\omega)}\right|_{\omega=\omega_{\mathrm{ssc}}} (\sigma^* + j\Delta\omega^*) \\
&= R(j\omega_{\mathrm{ssc}}) + 0 - j\left[\left.\frac{dR(j\omega)}{d\omega}\right|_{\omega=\omega_{\mathrm{ssc}}} + j\left.\frac{dX(j\omega)}{d\omega}\right|_{\omega=\omega_{\mathrm{ssc}}}\right] \\
&\quad \times(\sigma^* + j\Delta\omega^*) \\
&= \left[R(j\omega_{\mathrm{ssc}}) + \left.\frac{dX(j\omega)}{d\omega}\right|_{\omega=\omega_{\mathrm{ssc}}} \sigma^* + \left.\frac{dR(j\omega)}{d\omega}\right|_{\omega=\omega_{\mathrm{ssc}}} \Delta\omega^*\right] \\
&\quad + j\left[\left.\frac{dR(j\omega)}{d\omega}\right|_{\omega=\omega_{\mathrm{ssc}}} \sigma^* - \left.\frac{dX(j\omega)}{d\omega}\right|_{\omega=\omega_{\mathrm{ssc}}} \Delta\omega^*\right] \qquad (17)
\end{aligned}
$$

Therefore, the following formulas hold for all $s* = \sigma^* + j\omega^*$ with $||(\sigma^* + j\omega^*) - j\omega_{\mathrm{ssc}}|| < \delta$:

$$
\begin{cases}
R(j\omega_{\mathrm{ssc}}) + B\sigma^* + A\Delta\omega^* = 0 \\
A\sigma^* - B\Delta\omega^* = 0
\end{cases} \qquad (18)
$$

where

$$
A = \left.\frac{dR(j\omega)}{d\omega}\right|_{\omega=\omega_{\mathrm{ssc}}}, \; B = \left.\frac{dX(j\omega)}{d\omega}\right|_{\omega=\omega_{\mathrm{ssc}}}. \qquad (19)
$$

By solving (18), it yields that

$$
\begin{cases}
\sigma^* = \frac{-B}{A^2+B^2} R(j\omega_{\mathrm{ssc}}) \\
\Delta\omega^* = \frac{A}{B}\sigma^*
\end{cases}. \qquad (20)
$$

Considering (20) and $\sigma^* \ll \omega^*$, so $\Delta\omega^* \ll \omega^*$. As a result,

$$
\omega^* \simeq \omega_{\mathrm{ssc}}. \qquad (21)
$$

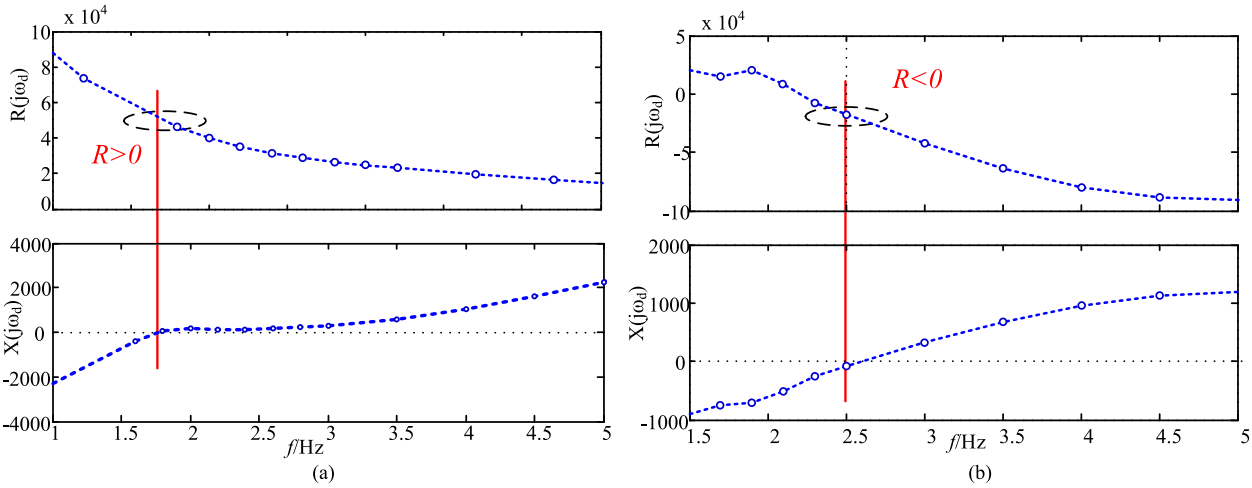

Fig. 14. Impedance—frequency curves of the determinant $\boldsymbol{D(j\omega_d)}$ (a) STATCOM #1 is ON; (b) STATCOMs #1 and 2 are ON.

TABLE III
COMPARISIONS OF THE OSCILLATION FREQUENCY AND AMPLITUDE AT DIFFERENT STAGES

Methods		Subsynchronous components		Super-synchronous components	
		Freq./Hz	Amp./kA	Freq./Hz	Amp./kA
IM-based analysis		2.46	/	97.54	/
Nonlinear	$t = 1$ s (not clipped yet)	2.46	0.011	97.54	0.026
EMT	$t = 1.4$ s (clipped)	2.50	0.010	97.50	0.025
simulations	without limiter	2.46	0.011	97.54	0.026

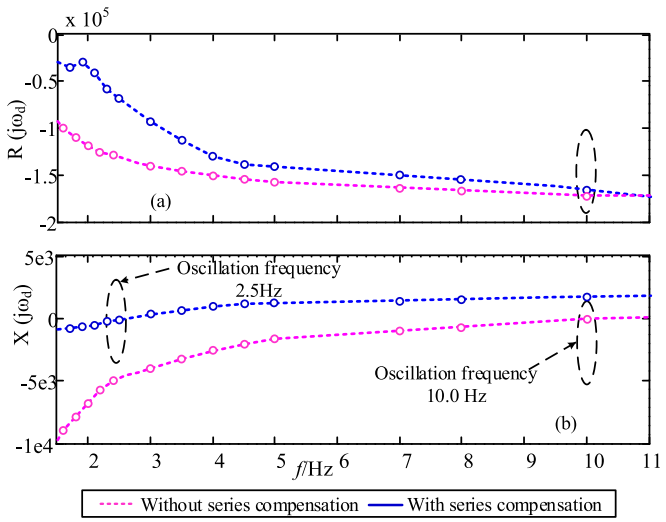

Fig. 15. Impedance—frequency curves of the determinant $\boldsymbol{D(j\omega_d)}$ with and without series compensation.

According to (20), the stability or damping of the S^{2}SI mode characterized by σ^* can be judged by the polarity of $R(j\omega_{\rm ssc})$ and the slope of $X(j\omega)$ at the zero-crossing point, or $B = [dX(j\omega)/d\omega]_{\omega=\omega_{\rm ssc}}$. Specifically, if the product of $R(j\omega_{\rm ssc})$ and B is negative, σ^* will be positive, indicating an unstable SSI and vice visa. Meanwhile, (21) indicates that the oscillation frequency of the S^{2}SI can be approximated by the zero-crossing point of the imaginary part of the determinant.

To sum up, if there is an S^{2}SI mode in the system and the damping is much smaller than the oscillation frequency, the characteristics of the S^{2}SI mode can be evaluated by the following criterion [40], [41].

1) Its frequency is approximated by one of the zero-crossing points of $X(j\omega)$, or $X(j\omega_{\rm ssc}) = 0$.
2) Its stability or damping is jointly determined by $R(j\omega)$ and the slope of $X(j\omega)$ around $\omega_{\rm ssc}$: If $X(j\omega)$ crosses the zero-axis with a positive slope (meaning from capacitive to inductive), a positive (negative) resistance at the zero-crossing point, or $R(j\omega_{\rm ssc}) > 0$ (< 0), predicts a (an) stable (unstable) S^{2}SI; otherwise, if the slope is negative, the conclusion will be reversed correspondingly.

D. IM-Based Analysis of the Actual S^{2}SI Incident

For the target system, the S^{2}SC-IMs of the STATCOM ($Z_S(j\omega_{\rm d})$), the HVDC ($Z_H(j\omega_{\rm d})$), and the weak AC grid ($Z_A(j\omega_{\rm d})$) are measured under the operating condition corresponding to the real S^{2}SI incident. The total S^{2}SC-IM ($Z_\Sigma(j\omega_{\rm d})$) is then calculated using (7). The frequency-dependent characteristics of all IMs are displayed in Figs. 12 and 13, from which the following can be observed.

1) The impedance of HVDC is much larger than those of other components (its value is divided by 1000 to be

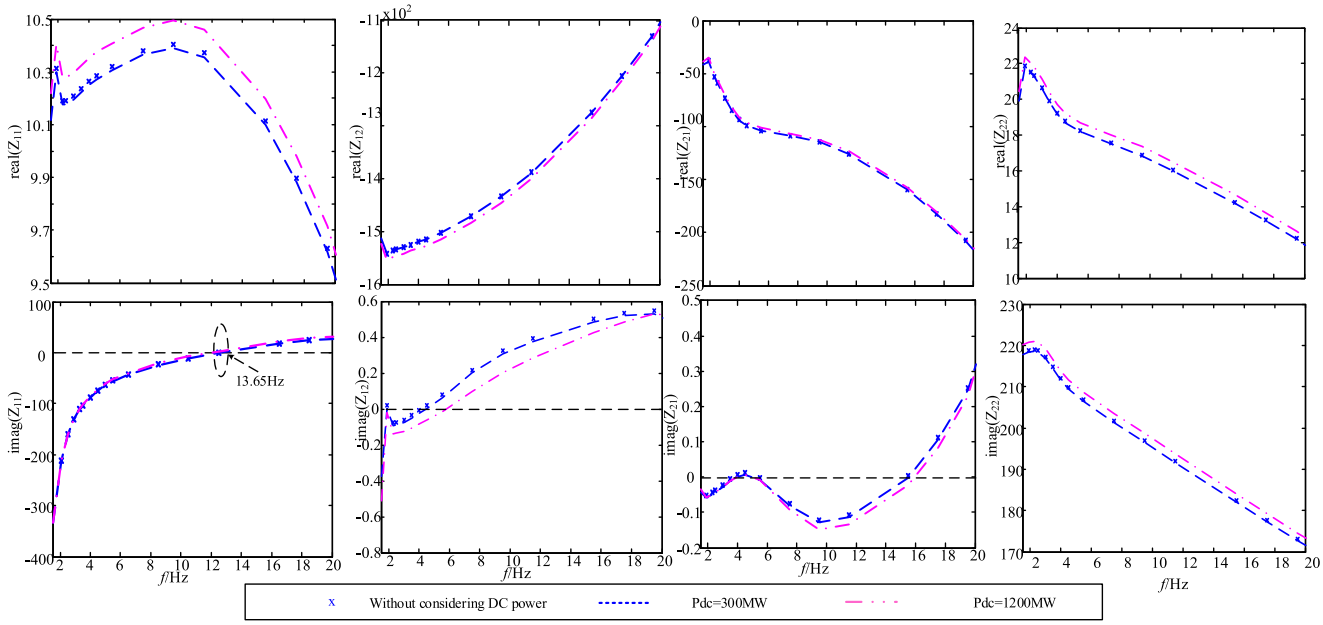

Fig. 16. Impedance—frequency curves of the total impedance with/without considering the DC power.

shown in Fig. 12), which indicates that HVDC does not participated into the oscillation so much.

2) The mutual impedance of the AC grid is almost zero, whereas the mutual impedances of the STATCOM and the HVDC are nonzero values, which means that the former has little sub- and super-synchronous coupling effects but the latter two have obvious coupling effects.
3) The mutual impedances ($Z_{12}(j\omega_{\rm d})$ and $Z_{21}(j\omega_{\rm d})$) of STATCOM exhibit capacitive reactance and negative resistance in a certain range of frequency.

Fig. 14 shows the frequency characteristics of the determinant or $D(j\omega_d)$ of the total S^{2}SC-IM. For comparison, the cases of one and two STATCOMs are displayed side by side. For the one-STATCOM case [see Fig. 14(a)], $X(j\omega_d)$ crosses the zero axis at around 1.75 Hz with a positive slope, and the corresponding $R(j\omega_d)$ is greater than zero, which, according to the stability criterion, means the S^{2}SI is stable. On the contrary, the two-STATCOM case [see Fig. 14(b)] has a negative resistance at the zero-crossing point (2.46 Hz) of the reactance, indicating an unstable S^{2}SI. This observation derived from the S^{2}SC-IM is consistent with the field measurements as well as the time-domain simulations. Thus, the effectiveness of IM-based analysis is verified.

The consistency between the proposed IM-based method and the nonlinear EMT simulations is further illustrated in Table III. With the IM-based analysis, the sub-/super-synchronous frequencies of the S^{2}SI are obtained as 2.46/97.54 Hz, respectively. In the nonlinear EMT simulations, "$t = 1$ s" corresponds to the time when i_{qr} has not yet been clipped; "$t = 1.4$ s" corresponds to the time when i_{qr} has been clipped slightly; "without limiter" corresponds to the results with the limiter cancelled deliberately. The simulation results show that the frequencies/amplitudes of oscillation before, after, and without the clipping of i_{qr} are very close. For instance, the frequency deviation is less than 0.05 Hz. Actually there is only very shallow saturation during the oscillation events, and it would not cause major difference in oscillation frequency or amplitude. As shown in Table III, the results of the IM-based analyses are consistent with those of the EMT simulations (before, after, and without signal clipping). Therefore, it can be concluded that the proposed stability criterion based on S^{2}SC-IM is able to predict the stability as well as the approximate frequency of the oscillations.

E. IM-Based Investigation of the Impacts From the Various Factors

In this section, the impacts on S^{2}SI from the various factors are confirmed and further quantified using the IM-based analysis.

1) Impact From the Number of Online STATCOMs: Besides the results shown in Fig. 13, the cases of none and three STATCOMs have also been similarly investigated. The conclusions are the same as those drawn from EMT simulations (see Section III-B): When there is no or only one STATCOM in service, the resistance at the zero-crossing frequency, or $\boldsymbol{R(j\omega_{\rm sub})}$, is positive, indicating stable S^{2}SI. However, if two or more STATCOMs are grid-connected, $\boldsymbol{R(j\omega_{\rm sub})}$ would become negative and thus result in an unstable S^{2}SI.

2) Impact From the Status of Series Compensation: Fig. 15 shows the curves of $R(j\omega_d)$ and $X(j\omega_d)$ for the in service/out of service status of the series compensation. It is seen that the bypass of the series compensation does not eliminate the oscillation but alters its frequency. The zero-crossing point of $X(j\omega_d)$ is increased to around 10.0 Hz. Noticeably, the resistance $R(j\omega_d)$ at the new oscillation frequency is more negative, which implies that the damping is worsen and the oscillation would become more severe. This IM-based observation is fairly confirmed by the simulation results presented in Section III-B

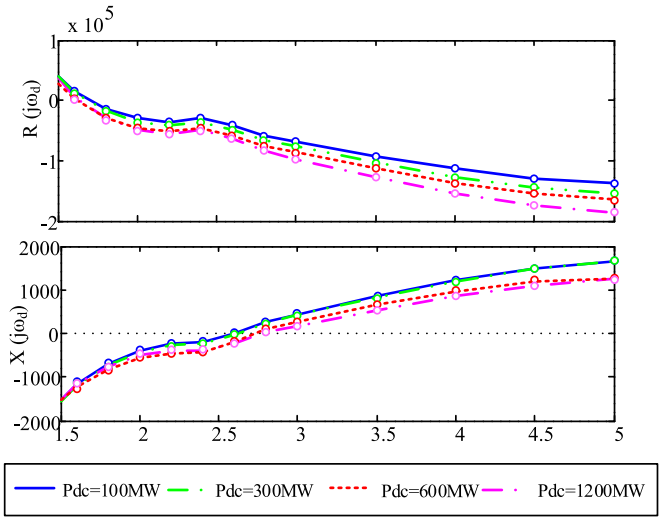

Fig. 17. Impedance—frequency curves of the determinant $\boldsymbol{D(j\omega_d)}$ with varying DC power.

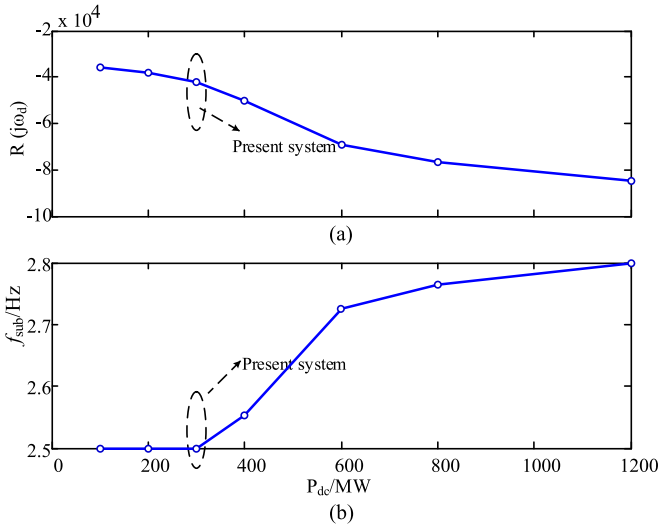

Fig. 18. Oscillation frequencies and the corresponding resistance at different loading levels of HVDC.

and once again shows that the oscillation is not caused by the series compensation.

3) Impact From the Loading Level of HVDC: The total impedances with and without considering the impedance of HVDC are shown in Fig. 16. The "x" marked line stands for the situation without incorporating the impedance of HVDC; whereas the dashed lines denoted as "$P_{\rm dc} = 300$ MW" and "$P_{\rm dc} = 1200$ MW" stand for the situation with the impedance of HVDC considered, and the DC power being 300 and 1200 MW, respectively. The relatively low DC power (300 MW) corresponds to the case when the actual S^{2}SI event happened; whereas high DC power (1200 MW) corresponds to the maximum allowable DC power for the contingency situation with only a single line in service from FN to WP (Part C). Obviously, when the DC powers is relatively low, for instance no more than 300 MW, the total impedances with and without the impedance of HVDC almost coincide, which means the latter has very little impact on the former. When the DC power is relatively large, the impedance of HVDC would bring some difference to the total impedance. In other words, the HVDC has a slight impact on the S^{2}SI.

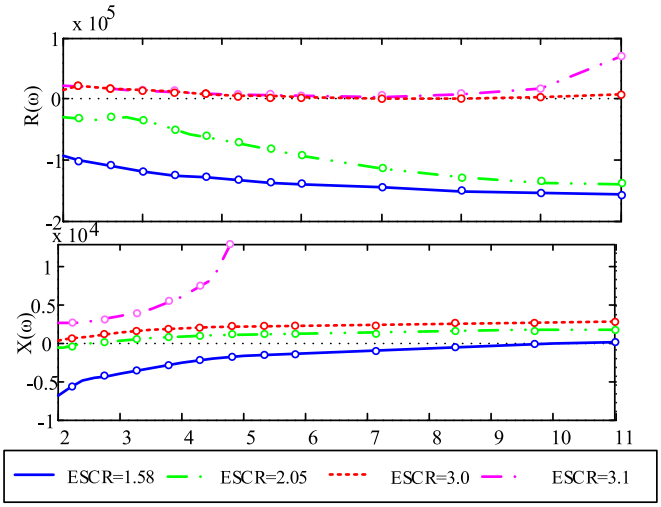

Fig. 19. Impedance—frequency curves of the determinant $\boldsymbol{D(j\omega_d)}$ with varying ESCR.

Furthermore, the real and imaginary parts of $D(j\omega_d)$ at different loading levels of HVDC are displayed in Fig. 17. And the relationship between the critical resistance/the oscillation frequency and the variation of the HVDC power is illustrated in Fig. 18. It can be seen that when the DC power is at a very low loading level ($< 10\%$ of its rated power), the oscillation frequency remains almost unchanged. This is because the impedance of HVDC is much larger than those of other components (see Fig. 13), and HVDC does not participated into the oscillation so much. If the DC power is increased above 10% of its rated power, the subsynchronous frequency will rise slightly. Meanwhile, since the S^{2}SC-IM of HVDC decreases, the S^{2}SI-IM of total S^{2}SC-IM ($\boldsymbol{Z_\Sigma(j\omega_d)}$) decreases a bit, resulting in the increased amplitude of the S^{2}SI. Therefore, the variation of the HVDC power will not determine the occurrence of the S^{2}SI. The increased HVDC power only lead to a slightly rise of the subsynchronous frequency and drop of the resistance $R(j\omega_d)$.

4) Impact From the Strength of the AC System: The real and imaginary parts of $D(j\omega_d)$ under typical ESCRs are demonstrated in Fig. 19. Therein, "ESCR $= 1.58$" is the leftmost point in Fig. 20; "ESCR $= 2.05$" corresponds to the ESCR of the actual S^{2}SI events; "ESCR $= 3.0$" is the critical point of no-zero crossing, etc. Furthermore, Fig. 20 clearly shows the relationships between the ESCR and the critical resistance/the oscillation frequency. As can be seen, when the ESCR of the system is increased, the oscillation frequency will drop gradually. Simultaneously, the system damping will be increased, resulting in the drop of the amplitude of the S^{2}SI. Noticeably, when the ESCR is above 3.0, there is no zero-crossing, which indicates no occurrence of the S^{2}SI. Moreover, $R(j\omega_d)$ is positive and provides positive damping for the S^{2}SI. Therefore, it is concluded that with the increase of the strength of the system, the adverse S^{2}SI phenomenon can be mitigated or even resolved.

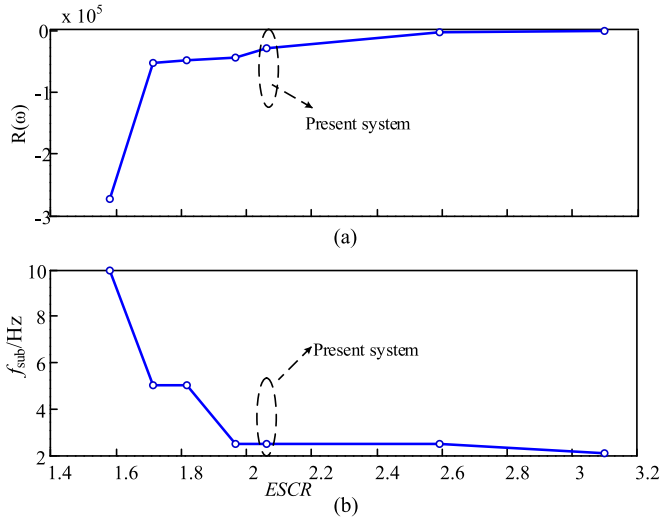

Fig. 20. Curves of critical resistance and oscillation frequency under different strength of the system.

V. Conclusion

The oscillation incidents that occurred in CSG have demonstrated a different type of interaction, namely S^2SI between VSC-based STATCOMs and a weak AC grid. Its striking feature lies in the strong coupling effect of sub- and super-synchronous components. The proposed S^2SC-IM represents such a coupled interaction and lays the foundation for the establishment of a stability criterion. Field measurements are evaluated and EMT simulations as well as S^2SC-IM-based theoretical analyses are carried out to clarify the characteristics of the S^2SI event. The main influential factors are identified and their impacts on S^2SI are summarized as follows:

1) The power oscillations are mainly caused by the dynamic interaction between STATCOMs and the weak grid. The number of online STATCOMs and the strength of the system have significant impacts on the S^2SI. However, the status of the series compensation and HVDC has a relatively minor effect.
2) For the studied system, if two or more STATCOMs are grid-connected, unstable S^2SI would be excited, especially when the AC grid is weakened during contingencies. An increase of ESCR indicates a decrease of the oscillation frequency and an improvement of resistance or damping. An ESCR above 3.0 would avoid unstable S^2SI completely.
3) Neither the loading level of HVDC nor the switching ON/OFF of series compensations will determine the existence or non-existence of S^2SI, but they only have slight effect on the oscillation magnitude and frequency.

References

[1] H. Wang, M. Wu, and J. Sun, "Analysis of low-frequency oscillation in electric railways based on small-signal modeling of vehicle-grid system in dq frame," *IEEE Trans. Power Electron.*, vol. 30, no. 9, pp. 5318–5330, Sep. 2015.

[2] Y. Yu *et al.*, "Oscillation energy analysis of inter-area low-frequency oscillations in power systems," *IEEE Trans. Power Syst.*, vol. 31, no. 2, pp. 1195–1203, Mar. 2016.

[3] D. Shu, X. Xie, V. Dinavahi, C. Zhang, X. Ye, and Q. Jiang, "Dynamic phasor based interface model for EMT and transient stability hybrid simulations," *IEEE Trans. Power Syst.*, vol. PP, no. 99, 2017.

[4] Z. Bo *et al.*, "Developments of power system protection and control," *Protection Control Modern Power Syst.*, vol. 1, no. 1, pp. 1–8, 2016.

[5] P. Channegowda and V. John, "Filter optimization for grid interactive voltage source inverters," *IEEE Trans. Ind. Electron.*, vol. 57, no. 12, pp. 4106–4114, Dec. 2010.

[6] T. Abeyasekera, C. M. Johnson, D. J. Atkinson, and M. Armstrong, "Suppression of line voltage related distortion in current controlled grid connected inverters," *IEEE Trans. Power Electron.*, vol. 20, no. 6, pp. 1393–1401, Nov. 2005.

[7] K. M. Alawasa, Y. A. R. I. Mohamed, and W. Xu, "Active mitigation of sub-synchronous interactions between PWM voltage-source converters and power networks," *IEEE Trans. Power Electron.*, vol. 29, no. 1, pp. 121–134, Jan. 2014.

[8] L. Wang, X. Xie, Q. Jiang, H. Liu, Y. Li, and H. Liu, "Investigation of SSR in practical DFIG-based wind farms connected to a series-compensated power system," *IEEE Trans. Power Syst.*, vol. 30, no. 5, pp. 2772–2779, Sep. 2015.

[9] L. Fan and Z. Miao, "Mitigating SSR using DFIG-based wind generation," *IEEE Trans. Sustain. Energy*, vol. 3, no. 3, pp. 349–358, Jul. 2012.

[10] K. M. Alawasa, Y. A.-R. I. Mohamed, and W. Xu, "Active mitigation of sub-synchronous interactions between PWM voltage-source converters and power networks," *IEEE Trans. Power Electron.*, vol. 29, no. 1, pp. 121–134, Jan. 2014.

[11] L. Harnefors, M. Bongiorno, and S. Lundberg, "Input-admittance calculation and shaping for controlled voltage-source converters," *IEEE Trans. Ind. Electron.*, vol. 54, no. 6, pp. 3323–3334, Dec. 2007.

[12] L. Xu and L. Fan, "Impedance-based resonance analysis in a VSC-HVDC system," *IEEE Trans. Power Del.*, vol. 28, no. 4, pp. 2209–2216, Oct. 2013.

[13] J. Sun, "Small-signal methods for AC distributed power systems—A Review," *IEEE Trans. Power Electron.*, vol. 24, no. 11, pp. 2545–2554, Nov. 2009.

[14] Z. Liu, J. Liu, X. Hou, Q. Dou, and T. Liu, "Output impedance modeling and stability prediction of three-phase paralleled inverters with master-slave sharing scheme based on terminal characteristics of individual inverters," *IEEE Trans. Power Electron.*, vol. 31, no. 7, pp. 5306–5320, Jul. 2016.

[15] K. Pietilainen, L. Harnefors, A. Petersson, and H. P. Nee, "DC-link stabilization and voltage sag ride-through of inverters drives," *IEEE Trans. Ind. Electron.*, vol. 53, no. 4, pp. 1261–1268, Jun. 2006.

[16] Y. Huang, X. Yuan, J. Hu, and P. Zhou, "Modeling of VSC connected to weak grid for stability analysis of DC-link voltage control," *IEEE J. Emerg. Sel. Topics Power Electron.*, vol. 3, no. 3, pp. 1193–1204, Dec. 2015.

[17] Y. Song, X. Wang, and F. Blaabjerg, "High-Frequency resonance damping of DFIG-based wind power system under weak network," *IEEE Trans. Power Electron.*, vol. 32, no. 3, pp. 1927–1940, Mar. 2017.

[18] H. Liu, X. Xie, C. Zhang, Y. Li, H. Liu, and Y. Hu, "Quantitative SSR analysis of series-compensated DFIG-based wind farms using aggregated RLC circuit model," *IEEE Trans. Power Syst.*, vol. 32, no. 1, pp. 474–483, Jan. 2017.

[19] L. Fan, C. Zhu, Z. Miao, and M. Hu, "Modal analysis of a DFIG-based wind farm interfaced with a series compensated network," *IEEE Trans. Energy Convers.*, vol. 26, no. 4, pp. 1010–1020, Dec. 2011.

[20] L. Fan, R. Kavasseri, Z. Miao, and C. Zhu, "Modeling of DFIG-based wind farms for SSR analysis," *IEEE Trans. Power Del.*, vol. 25, no. 4, pp. 2073–2082, Oct. 2010.

[21] H. Liu and J. Sun, "Voltage stability and control of offshore wind farms with AC collection and HVDC transmission," *IEEE J. Emerg. Sel. Topics Power Electron.*, vol. 2, no. 4, pp. 1181–1189, Dec. 2014.

[22] H. Liu *et al.*, "Subsynchronous interaction between direct-drive PMSG based wind farms and weak AC networks," *IEEE Trans. Power Syst.*, vol. 32, no. 6, pp. 4708–4720, Nov. 2017.

[23] A. Platzker and W. Struble, "Rigorous determination of the stability of linear n-node circuits from network determinants and the appropriate role of the stability factor K of their reduced two-ports," *Proc. 3rd Int. Workshop Integrated Nonlinear Microw. Millimeterwave Circuits*, Oct. 1994, pp. 93–107.

[24] *IEEE Guide for Planning DC Links Terminating at AC Locations Having Low Short-Circuit Capacities*," IEEE Std. 1204-1997, Jan. 21, 1997, pp. 1–216.

[25] E. Eitelberg, J. C. Balda, E. S. Boje, and R. G. Harley, "Stabilizing SSR oscillations with a shunt reactor controller for uncertain levels of series compensation," *IEEE Trans. Power Syst.*, vol. PS-3, no. 3, pp. 936–943, Aug. 1988.
[26] C. Guo, C. Li, C. Zhao, X. Ni, K. Zha, and W. Xu, "An evolutional line-commutated converter integrated with thyristor-based full-bridge module to mitigate the commutation failure," *IEEE Trans. Power Electron.*, vol. 32, no. 2, pp. 967–976, Feb. 2017.
[27] C. Guo, Y. Liu, C. Zhao, X. Wei, and W. Xu, "Power component fault detection method and improved current order limiter control for commutation failure mitigation in HVDC," *IEEE Trans. Power Del.*, vol. 30, no. 3, pp. 1585–1593, Jun. 2015.
[28] M. Belkhayat, "Stability criteria for AC power systems with regulated loads," Ph.D. dissertation, dept. Elect. Eng., Purdue Univ., West Lafayette, IN, USA, Dec. 1997.
[29] J. Sun, "Small-signal methods for AC distributed power systems," *IEEE Trans. Power Electron.*, vol. 24, no. 11, pp. 2545–2554, Nov. 2009.
[30] M. Cespedes and J. Sun, "Modeling and mitigation of harmonic resonance between wind turbines and the grid," in *Proc. IEEE Energy Convers. Congr. Expo.*, Sep. 2011, pp. 2109–2116
[31] M. Cespedes and J. Sun, "Impedance modeling and analysis of grid-connected voltage-source converters," *IEEE Trans. Power Electron.*, vol. 29, no. 3, pp. 1254–1261, Mar. 2014.
[32] Z. Liu, J. J. Liu, W. H. Bao, and Y. L. Zhao, "Infinity-norm of impedance based stability criterion for three-phase AC distributed power systems with constant power loads," *IEEE Trans. Power Electron.*, vol. 30, no. 6, pp. 3030–3043, Jun. 2015.
[33] X. Wang, L. Harnefors, and F. Blaabjerg, "Unified impedance model of grid-connected voltage-source converters," *IEEE Trans. Power Electron.*, vol. 33, no. 2, 2018.
[34] M. Mohades, A. M. Gole, and S. Elez, "Steady state frequency response of StatCom," *IEEE Trans. Power Del.*, vol. 16, no. 1, pp. 18–23, Jan. 2001.
[35] M. K. Bakhshizadeh, X. Wang, F. Blaabjerg, L. Kocewiak, C. L. Bak, and B. Hesselbak, "Coupling in phase domain impedance modelling of grid-connected converters," *IEEE Trans. Power Electron.*, vol. 31, no. 10, pp. 6792–6796, Oct. 2016.
[36] H. Yi, X. Wang, F. Blaabjerg, and F. Zhuo, "Impedance analysis of SOGI-FLL-based grid synchronization," *IEEE Trans. Power Electron.*, vol. 32, no. 10, pp. 7409–7413, Oct. 2017.
[37] S. Shah and L. Parsa, "Impedance modeling of three-phase voltage source converters in DQ, sequence, and phasor domains," *IEEE Trans. Energy Convers.*, vol. 32, no. 3, pp. 1139–1150, Sep. 2017.
[38] Z. Miao, "Impact of unbalance on electrical and torsional resonances in power electronic interfaced wind energy systems," *IEEE Trans. Power Syst.*, vol. 28, no. 3, pp. 3105–3113, Aug. 2013.
[39] L. Harnefors, M. Bongiorno, and S. Lundberg, "Input-admittance calculation and shaping for controlled voltage-source converters," *IEEE Trans. Ind. Electron.*, vol. 54, no. 6, pp. 3323–3334, Dec. 2007.
[40] A. Tabesh and R. Iravani, "On the application of the complex torque coefficients method to the analysis of torsional dynamics," *IEEE Trans. Energy Convers.*, vol. 20, no. 2, pp. 268–275, Jun. 2005.
[41] L. Xu and L. Fan, "Impedance-based resonance analysis in a VSC-HVDC system," *IEEE Trans. Power Del.*, vol. 28, no. 4, pp. 2209–2216, Oct. 2013.

Dewu Shu (S'14) received the B.Sc. degree in electrical engineering from Tsinghua University, Beijing, China, in 2013. He is currently working toward the Ph.D. degree in the Department of Electrical Engineering, Tsinghua University.

His research interests include stability of power electronics, parallel and distributed computing.

Xiaorong Xie (M'02–SM'14) received the B.Sc. degree in electrical engineering from Shanghai Jiao Tong University, Shanghai, China, in 1996, and the Ph.D./M. Eng. degrees from Tsinghua University, Beijing, China, in 2001.

From 2001 to 2005, he was a Lecturer with the Department of Electrical Engineering, Tsinghua University. Since 2005, he works as an Associate Professor in the same department. His current research interests focus on power system analysis and control, and flexible AC transmission systems.

Hong Rao (SM'12) received the B.Sc. degree in electrical engineering from Huazhong University of Science Technology, Wuhan, China, in 1982.

Currently, he is with the Electric Power Research Institute, China Southern Power Grid, Guangzhou, China. His research activities include HVDC technology as well as power system analysis and stability.

Xiaodan Gao (S'13) received the bachelor's degree in wind energy and power engineering from North China Electric Power University, Beijing, China, in 2013. She is currently working toward the Ph.D. degree in the Centre for Intelligent Electricity Networks, the University of Newcastle, Callaghan, NSW, Australia.

Her research interest includes wind power integration, wind turbine control, energy storage systems, and distribution system control.

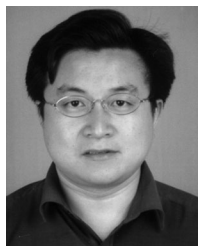

Qirong Jiang (M'98) received the B.S. and Ph.D. degrees in electrical engineering from Tsinghua University, Beijing, China, in 1992 and 1997, respectively.

Since 2006, he has been a Professor at Tsinghua University. His research interests include power system analysis and control, modeling and control of flexible AC transmission systems, power quality analysis and mitigation, power-electronic equipment, and renewable energy power conversion.

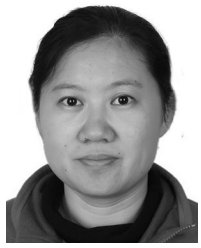

Ying Huang received the B.S. degree in electrical engineering from Shandong Polytechnic University, Jinan, China, in 1999, the M.S. degree electrical engineering from Shandong University, Jinan, China, in 2002, and the Ph.D degree in electrical engineering from Zhejiang University, Hangzhou, China, in 2005.

She is currently with the Electric Power Research Institute, China Southern Power Grid, Guangzhou, China. Her research interests include HVDC technology as well as audible noise control technology in converter station.